Breakdown of the Kondo insulating state in SmB_6 by introducing Sm vacancies

Michael E. Valentine,[1] Seyed Koohpayeh,[1] W. Adam Phelan,[1] Tyrel M. McQueen,[1]
Priscila F. S. Rosa,[2] Zachary Fisk,[2] and Natalia Drichko[1,*]

[1]*Institute for Quantum Matter and Department of Physics and Astronomy, Johns Hopkins University, Baltimore, Maryland 21218, USA*
[2]*Department of Physics and Astronomy, University of California, Irvine, California 92697, USA*

(Received 11 January 2016; revised manuscript received 14 July 2016; published 1 August 2016)

We explore the stability of the hybridization gap in SmB_6 to the presence of a small number of Sm vacancies typical for this material, and demonstrate the extreme fragility of the Kondo insulating state. For the most stoichiometric sample we detect the hybridization gap which appears below 50 K as a depressed electronic Raman intensity below about 30 meV. The spectral weight that shifts to higher frequencies on the opening of the hybridization gap forms two electronic maxima at 100 and 41 meV. We assign these maxima to the excitations between hybridized $4f$-$5d$ bands using recent band structure calculations. Below 30 K, in-gap exciton modes with long lifetimes protected by the hybridization gap develop at 16–18 meV. With the increase of the number of Sm vacancies the exciton features broaden, evidencing a decrease in the lifetime due to the presence of electronic states in the gap. At a concentration of Sm vacancies of only about 1% the in-gap exciton is completely quenched, and the hybridization gap is not fully opened. We suggest that only the most stoichiometric SmB_6 samples possess a bulk gap necessary for the topological Kondo insulator state.

DOI: 10.1103/PhysRevB.94.075102

I. INTRODUCTION

Much recent research is aimed at experimental realization of the topological insulator (TI) state of matter where topologically protected metallic surface states appear due to a surface crossing of inverted bulk bands. While the TI state has already been observed in band insulators, it is proposed that the strong electronic interactions in Kondo insulators could be a source of topological surface states [1–3]. SmB_6, which has been studied extensively for its mixed valence and Kondo insulating properties [4,5], is the prime candidate for a topological Kondo insulator (TKI). The presence of metallic surface states reveals itself as a plateau in the dc resistivity temperature dependence below 5 K [6–8]. Interpretation of these metallic surface states varies from topologically protected [6,8] to polarity-driven "trivial" surface states [9].

A requirement for a TI state is the presence of a bulk insulating gap with an inversion of bands. SmB_6 has been claimed to be the first topological insulator candidate with a truly insulating bulk [10]. In SmB_6, a gap opens at the Fermi level due to hybridization between $4f$ and $5d$ electronic bands below 70 K (below 150 K according to Ref. [11]). The Kondo insulating gap has been detected experimentally using a variety of different methods [6,11–17]. Band structure calculations predict a gap opening due to hybridization with band inversion necessary for topological nontriviality at the X point in the Brillouin zone (BZ) [3,18,19]. Indeed, a neutron scattering study [20] gives evidence of band inversion at the X and R points of the Brillouin zone (BZ).

On the other hand, there is some controversy regarding the bulk properties of SmB_6, and if they would allow the TKI state. For example, the shape and the offset temperature of the plateau, as well as the ratio of resistivity $\rho(2\text{ K})/\rho(300\text{ K})$ which characterizes the bulk insulating state, can differ between the samples due to defects and vacancies. In particular, the presence of a small number of Sm vacancies is typical for SmB_6 [21]. The evidence for metallic behavior in the bulk at temperatures relevant for TKI state is provided by 3D quantum oscillations [22].

In this work we show that the hybridization gap is extremely fragile to the presence of Sm vacancies. While the most stoichiometric samples demonstrate the presence of the gap, it starts to fill in with states at the concentration of vacancies below 1%. The presence of even 1% of Sm vacancies leads to smearing of the bulk hybridization gap in SmB_6 samples and would result in a breakdown of the TKI state.

We use Raman spectroscopy to probe the bulk hybridization gap in samples with the level of Sm vacancies up to 1%. In the same measurements we probe Sm-vacancy-induced phonon scattering, which independently characterizes the number of vacancies. Thus we provide the most reliable way to show a correlation between the number of Sm vacancies and the electronic properties.

II. EXPERIMENT

A. Crystal growth

In this study we used single crystals of SmB_6 grown by both Al flux and floating zone (FZ) techniques. For our study, we selected a crystal, referred to as Al Flux-SmB_6, found from Raman measurements to have the fewest Sm vacancies and comparable linewidths of boron Raman-active phonons for FZ samples. A value of the linewidth of boron phonons as a parameter to characterize the quality of SmB_6 samples and the degree of structural variation within Al-flux-grown samples will be discussed elsewhere [23].

FZ single crystals of SmB_6 were grown using the optical floating zone technique [7,21] and are representative of "typical" SmB_6 crystals described in these papers. An increasing presence of Sm vacancies along the length of a single FZ crystal occurs due to vaporization of the stoichiometric rod materials into a Sm-rich mixture and can be characterized by a systematic decrease in lattice parameters. For our study we used two samples cut from the most stoichiometric (FZ SmB_6-Pure) and most Sm-deficient (FZ SmB_6-Def) ends

*Corresponding author: drichko@jhu.edu

TABLE I. Polarizations of the measured Raman scattering spectra of SmB_6, the geometry of the measurements, and the probed irreducible representations for each polarization.

Polarization	e_i, e_s geometry	Symmetry (O_h)
(x,x)	$c(aa)\bar{c}$	$A_{1g} + E_g$
(x,y)	$c(ab)\bar{c}$	T_{2g}
(x',x')	$c\left(\frac{a+b}{\sqrt{2}}, \frac{a+b}{\sqrt{2}}\right)\bar{c}$	$A_{1g} + \frac{1}{4}E_g + T_{2g}$
(x',y')	$c\left(\frac{a+b}{\sqrt{2}}, \frac{a-b}{\sqrt{2}}\right)\bar{c}$	$\frac{3}{4}E_g$

of the rod. Based on powder diffraction measurements of the lattice parameters in comparison to previous results for nonstoichiometric SmB_6, we estimate the most deficient sample (FZ SmB_6-Def) to be about 1% deficient [21]. Magnetization measurements for the two FZ-grown samples did not show a significant difference in average magnetic moment which could arise from larger differences in the number of Sm vacancies [24].

B. Raman measurements

Raman measurements were performed using a Horiba Jobin-Yvon T64000 triple monochromator spectrometer in the pseudo-Brewster angle geometry for energies from 2.5 meV (20 cm^{-1}) to 500 meV (4000 cm^{-1}) with resolution up to 0.25 meV (2 cm^{-1}). A Coherent Ar^+ laser was used as a source for excitation light with wavelengths 488 nm and 514 nm which was focused on the samples with a spot size of 50 × 100 μm. Penetration depth of the light at 514 nm is estimated to be of the order of 100 nm. The measurements were performed on cleaved surfaces that were exposed to atmosphere. No Raman evidence of samarium oxide which typically appears on the surface of the samples exposed to air was detected in the measured Raman spectra.

Measurements were performed over a temperature range of 10 to 300 K using a Janis ST-500 cold finger cryostat; here the temperatures are corrected for the laser heating. All spectra were corrected by the Bose-Einstein thermal factor. To compare the results for different samples the spectra were normalized on the intensity of the 158 meV A_{1g} phonon to compensate for the small differences in intensity due to the variation in the quality of the cleaved surfaces.

SmB_6 has $Pm\bar{3}m$ cubic symmetry corresponding to O_h point group symmetry. The crystals were oriented using x-ray diffraction and polarization-dependent Raman scattering measurements. The temperature-dependent measurements were performed in the (100) plane with the orientations of the electrical field of the incident light e_i and electrical vector of the scattered light e_s listed in Table I. The large acceptance angle of the analyzing optics results in some additional signal from other polarizations. In the table we also present the irreducible representations of the O_h point group probed in these polarizations.

III. RESULTS

The Raman spectra of SmB_6 consist of relatively narrow phonon peaks superimposed on the electronic background. In Sec. III A, we discuss how previously unidentified defect-induced phonon scattering can be used to extract the information on Sm vacancies in the studied samples of SmB_6. In Sec. III B, the electronic Raman response for samples with different amounts of Sm vacancies is discussed.

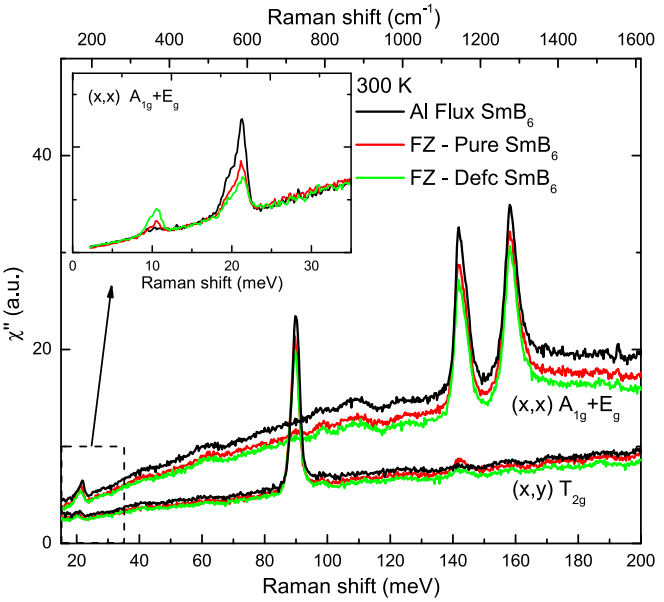

FIG. 1. Room temperature Raman spectra of the three studied SmB_6 samples with increasing number of Sm vacancies (Al Flux-SmB_6, FZ SmB_6-Pure, FZ SmB_6-Def, respectively) in (x,x) and (x,y) polarizations. The 3 first-order Raman-active phonons appearing at 89.6 meV (T_{2g}), 141.7 meV (E_g), and 158.3 meV (A_{1g}) are superimposed on a broad continuum of electronic scattering. Inset shows low-frequency (x,x) spectra of the samples. Two symmetry-forbidden peaks appear at 10 meV and 21 meV and correspond to defect-induced and two-phonon scattering, respectively.

A. Phonon scattering results

In the SmB_6 Raman spectra, the three symmetry-allowed Γ-point phonons seen as the intense relatively narrow features (Fig. 1) are the T_{2g} phonon at 89.6 meV (723 cm^{-1}), E_g at 141.7 meV (1143 cm^{-1}), and A_{1g} at 158.3 meV (1277 cm^{-1}), representing exclusively distortions of B_6 octahedra [25]. They are observed in polarizations corresponding to their symmetries and are well known from other vibrational Raman studies of SmB_6 crystals [25–29]. The relatively large linewidths of 2–4 meV emphasize the role of valence fluctuations and electron-phonon coupling. Al flux grown samples can show variations among the energies of these phonons by 1 meV [23], but for this work we chose a sample (Al Flux-SmB_6) with spectra where linewidths and energies match those of the FZ-grown samples. This exact coincidence of B_6 phonon lines for the studied samples ensures no difference in B_6 cage for these samples.

At energies well below the frequencies of distortions of B_6 octahedra, we observe features at 10 and 21 meV (see Fig. 1) with largest intensity in (x,x). Since phonon energies are proportional to $\frac{1}{\sqrt{m}}$ of the atoms involved, at these low frequencies we expect the collective motions of the Sm and B_6 centers. In the cubic unit cell of SmB_6, $Pm\bar{3}m$ space group, the Sm ion is located at a center of inversion

symmetry, and thus there are no allowed in first-order Raman scattering Γ-point phonons associated with Sm movement. We attribute the 10 meV feature to finite-momentum scattering from acoustic phonons Raman active due to local symmetry breaking induced by the presence of Sm defects. The loss of translational invariance allows light scattering from all points within the BZ [30] leading to a Raman intensity that depends on the density of states (DOS). Neutron scattering experiments [31] show a relatively flat dispersion of the acoustic phonon branches over the majority of the BZ which is responsible for the small linewidth of the Raman phonon line at 10 meV. While we would also expect the Raman scattering on the optical phonon branches at finite momenta due to Sm defects, the large dispersions of these branches would lead to a weak undistinguishable feature spanning a large energy range [31,32].

We base the correspondence between the number of Sm vacancies and intensity of the 10 meV phonon on data for the FZ-grown samples used in our study. For these samples the presence of Sm vacancies was estimated by measurements of the variation in lattice constants [21]. The Sm-defect-induced phonon at 10 meV shows an increase in spectral weight by about 1.5 times (Fig. 1) with an increase in Sm deficiency of less than 1% between the two FZ-grown samples. This demonstrates that Raman scattering can be effectively used to characterize the relative presence of Sm vacancies in SmB_6 samples. Moreover, in contrast to the estimation of the number of Sm vacancies by measurements of a lattice constant [21], inelastic light scattering probes the presence of defects on Sm sites directly. In our case care was taken to exclude other origins of defects on Sm cites by checking the elemental content of the samples by EDS measurements and mass spectrometry [21]. The intensity of the 10 meV phonon has nearly zero spectral weight for the Al Flux-SmB_6 sample used in this study, demonstrating that the sample has the lowest number of Sm vacancies. It is important to emphasize here that the presence of vacancies as was shown in [21] is individual for each sample and does not directly depend on FZ vs Al flux method of growth.

The 21 meV feature has a different origin, and thus shows a reverse dependence on the number of Sm defects at room temperature (see inset in Fig. 1). A comparison to neutron scattering spectra [32] suggests that it originates from two overlapping effects: two-phonon scattering from acoustic phonons and valence fluctuations coupled to the lattice deformation (exciton-polarons). For two-phonon overtone scattering from the acoustic branches ($A + A$), in agreement with the expectations [28,33,34] we observe the maximum intensity in A_{1g} polarization and a decrease in intensity on cooling as $(\frac{1}{1-e^{-\frac{\hbar\omega}{2kT}}})^2$. The origin of the untypically large strength of two-phonon scattering is phonon anomalies due to phonon coupling to d electrons [28,35,36]. In an imperfect crystal a matrix element which gives rise to the large two-phonon scattering is expected to decrease [36], explaining the decrease of the two-phonon feature on the increase of vacancies. In fact, both an increase of acoustic-phonon Raman-forbidden scattering and the decrease of two-phonon scattering on an increase of disorder was also observed for substoichiometric transition metal carbides [36].

The above analysis of phonon scattering associated with Sm atoms allows us to order the three studied samples by increasing number of Sm vacancies from Al Flux-SmB_6 to FZ SmB_6-Pure, and further to FZ SmB_6-Def. As the next step we follow the temperature dependence of electronic Raman scattering for these samples.

B. Electronic Raman scattering results

In the Raman spectra of all three samples at 300 K, we observe electronic background which linearly increases in intensity with energy up to about 150 meV (1200 cm^{-1}) and stays constant at higher energies (see Fig. 1). The background is observed in all four measured polarizations, though it is considerably weaker in (x,y). This background is present in the spectra excited with the 488 nm line as well, which suggests that it originates from electronic Raman scattering [37].

The changes observed in the Raman spectra of all the samples on cooling from 300 to 15 K are illustrated by the temperature dependence of the response of the FZ SmB_6-Pure sample in (x,x) polarization presented in Fig. 2(a). On

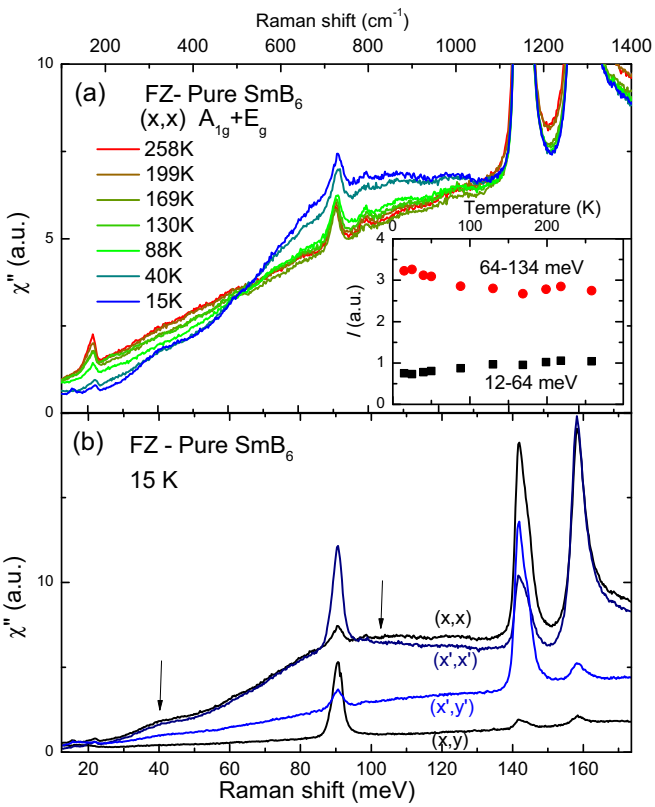

FIG. 2. (a) Temperature dependence of Raman spectra of the FZ SmB_6-Pure sample cooled from 300 K to 15 K in (x,x) polarization. Note redistribution of the spectral weight which occurs below 130 K to the frequencies above 100 meV, and below 50 K to the frequency range above 34 meV. The inset shows a temperature dependence of spectral weight $I(T) = \int_{\omega_1}^{\omega_0} \chi''(T,\omega)d\omega$ below ($\omega_0 =$ 12 meV, $\omega_1 = 64$ meV) and above ($\omega_0 = 64$ meV and $\omega_1 = 134$ meV) the isobestic point. (b) Raman spectra of FZ SmB_6-Pure sample at 15 K in $(x',y'),(x',x'),(x,y)$, and (x,x) polarizations; see Table I. The temperature-dependent response is most intense in (x',x') and (x,x) polarizations, suggesting that it belongs to A_{1g} symmetry.

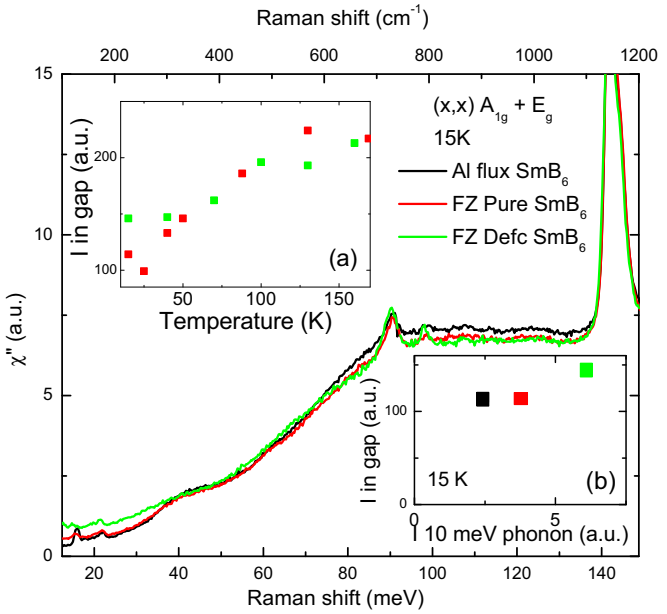

FIG. 3. Low-temperature Raman spectra of Al Flux-SmB_6, FZ SmB_6-Pure, and FZ SmB_6-Def samples at 15 K in (x,x) polarization. Note an increase of in-gap intensity and smearing of 41 meV feature with the increase in Sm vacancies. (a) Temperature dependence of the spectral weight $I(T) = \int_{\omega_1}^{\omega_0} \chi''(T,\omega)d\omega$ below 31.5 meV in FZ SmB_6-Pure sample (red dots) vs FZ SmB_6-Def sample (green dots). The difference becomes apparent below 50 K, where the 41 meV feature starts to develop in the spectra. (b) Spectral weight below 31.5 meV plotted against the intensity of the defect phonon. Note the increase of the low-frequency spectral weight with the increase of the number of Sm vacancies.

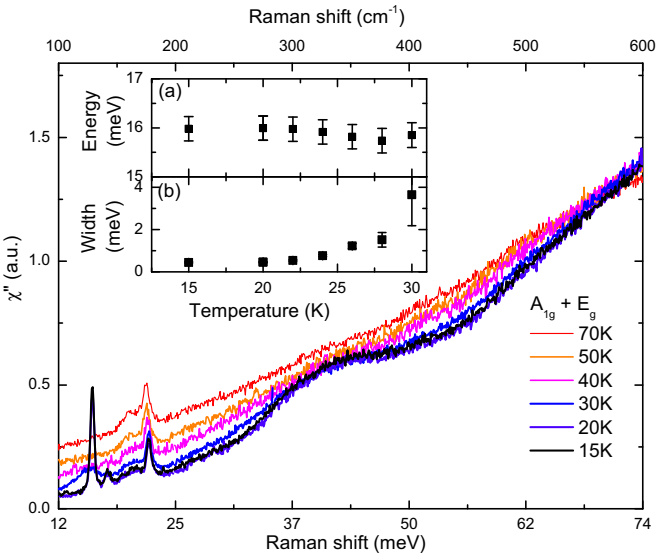

FIG. 4. Temperature dependence of the low-frequency Raman response of Al Flux-SmB_6 sample in (x,x) polarization. The exciton feature appears below 30 K at 16 meV. The inset shows a change of the position and width of the exciton on cooling.

decreasing temperatures below 130 K, we detect a spectral weight shift to frequencies above an isosbestic point of 64 meV. The resulting feature with a maximum at about 100 meV continues to develop down to 20 K. We follow the temperature dependence of the high-frequency feature in the inset of Fig. 3(a) by plotting the temperature dependence of the spectral weight $I(T) = \int_{\omega_1}^{\omega_0} \chi''(T,\omega)d\omega$ below ($\omega_0 = 12$ meV, $\omega_1 = 64$ meV) and above ($\omega_0 = 64$ meV and $\omega_1 = 134$ meV) the isosbestic point; $\chi''(T,\omega)$ is the Raman intensity in arbitrary units. Another shift of the spectral weight to higher frequencies occurs at temperatures below 50 K, resulting in a band at 41 meV with further suppression of the spectral weight below 34 meV. This lower-frequency effect is in general agreement with Refs. [27,28], while the feature at about 100 meV was not discussed. The total spectral weight of the spectra below 134 meV is conserved.

Polarization dependence of the spectra at 15 K [Fig. 2(b)] shows that both 100 meV and 41 meV maxima are most intense in (x,x) and (x',x'), with somewhat lower intensity at the same frequencies observed in (x',y'). This shows that both features appear in A_{1g} and E_g symmetries at the same energies. In T_{2g} symmetry [(x,y) polarization; see Sec. II B] the Raman response is low, featureless, and basically temperature independent.

Similar changes of the spectra on cooling are observed in the other samples. We compare the (x,x) spectra at 15 K for the samples with different concentrations of Sm vacancies in Fig. 3. The position and intensity of the feature at 100 meV is the same for all measured samples. At lower frequencies, for the FZ SmB_6-Def sample the 41 meV feature is smeared and the intensity at low frequencies is higher than in the spectra of the other two samples. The difference starts to develop below 50 K, where the samples with fewer Sm vacancies show a shift of spectral weight from low frequencies to the spectral region above about 31 meV, while no major changes occur for the FZ SmB_6-Def sample as follows from inset (a) in Fig. 3 where we plot a decrease of the spectral weight $I(T) = \int_{\omega_1}^{\omega_0} \chi''(T,\omega)d\omega$ between $\omega_0 = 11$ meV, $\omega_1 = 31.5$ meV on cooling for FZ SmB_6-Pure (red squares) and FZ SmB_6-Def (green squares). The correlation between the number of vacancies estimated as the intensity of the 10 meV phonon I(10 meV phonon) and the low-frequency spectral weight I(11–31 meV) [see inset (b), Fig. 3] shows the increase in low-frequency spectral weight on the increase of the number of vacancies to 1%.

For the Al Flux-SmB_6 sample at temperatures below 30 K we observe the developing of the sharp in-gap features in the range 16–18 meV. The temperature behavior followed in (x,x) polarization in Fig. 4 shows that the sharp peak forms when the spectral weight at low frequencies becomes sufficiently low. The frequency of the feature stays the same 16.0 meV, while the width decreases with temperature till it reaches the value of about 0.5 meV [see Fig. 4(b)]. At 20 K the temperature changes of the exciton features saturate. Table II lists all of the in-gap features observed at 15 K, including those in (x,y) polarization, and their symmetry assignment, which is in agreement with Refs. [27,28].

At 15 K in the spectra of the FZ SmB_6-Pure sample, lower intensity and a wider (1.7 meV) in-gap feature at 15.6 meV are superimposed on an even wider (4.7 meV) background.

TABLE II. Polarization dependence, symmetry, frequency, and width of the exitonic features observed in the samples with the smaller numbers of Sm vacancies (Al Flux-SmB_6 and FZ SmB_6-Pure) at 15 K.

		Al Flux		FZ Pure	
Polariz.	Symm.	Freq.	Width	Freq.	Width
(x,y)	T_{2g}	15.9 meV	0.7 meV		
(x,x)	E_g	16.0 meV	0.5 meV	15.6 meV	1.7 meV
(x,y)	T_{2g}	16.7 meV	0.7 meV		
(x,y)	T_{2g}	17.5 meV	0.7 meV	17.4 meV	1.5 meV

The in-gap excitations are not observed in the spectra of the FZ SmB_6-Def sample, where higher electronic scattering intensity is present at frequencies within the hybridization gap (Fig. 5).

IV. DISCUSSION

Observed in the electronic Raman response of SmB_6 shift of the spectral weight to higher frequencies on cooling and suppression of the intensity below about 30 meV clearly indicate the formation of the insulating gap. Theoretical calculations of the Raman response on an electronic-correlation-induced metal-insulator transition predict this behavior, and were discussed in connection with SmB_6 low-frequency Raman spectra [38]. The spectral weight of the Raman response is conserved below 134 meV (1080 cm^{-1}); this cutoff indicates the energy range associated with the low-temperature band structure formed due to hybridization of the orbitals. In the Raman spectra of the SmB_6 sample with the least number of Sm vacancies we observe two electronic maxima at 100 and 41 meV appearing at 130 and 50 K. For both features it yields 2Δ of about $6k_BT$, these values being close to each other and high as expected for strong electronic correlations [39].

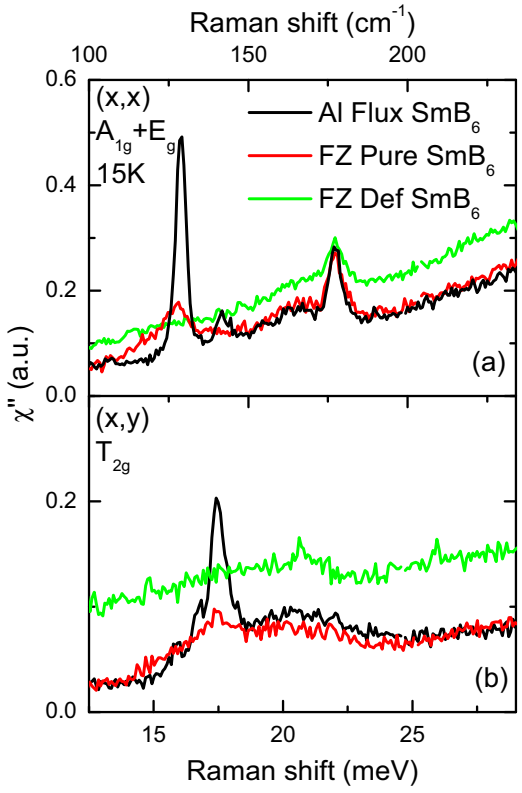

FIG. 5. Raman spectra in the frequency range of the exiton feature at 15 K for the measured samples, Al Flux-SmB_6, FZ SmB_6-Pure, and FZ SmB_6-Def in (x,x) polarization (a) and (x,y) polarization (b).

The observed polarization dependence confirms that the features in the spectra originate from electronic correlation effects. While the opening of the correlation-induced gap is expected to be observed in the A_{1g} and B_{1g} nonresonant response in D_{4h} symmetry (A_{1g} and E_g for O_h), in B_{2g} for D_{4h} symmetry in the approximation of cosine bands the nonresonant Raman response is predicted to be zero [39]. Indeed, in T_{2g} symmetry which can be projected on B_{2g} we see the lowest intensity electronic background and absence of the gap signatures [see Fig. 2(b)].

Electronic Raman scattering probes direct excitations at different parts of the BZ [40], where E_g probes the transitions around the X point, and A_{1g} probes the excitations over the whole BZ [39]. The interband excitations at 41 and 100 meV observed in our experiment at low temperatures correspond particularly well to the band structure calculations in Ref. [19]. These calculations predict a formation of a semiconductor-like gap with band inversion in the vicinity of the X point of the BZ as a result of hybridization of $5d$ and $4f$ bands, where the $4f$ $j = 5/2$ band splits into two Γ_7^f and one Γ_6^f band, suggesting two possible excitations to the upper unoccupied band at energies close to the values observed in our experiment. The flat dispersion of the relevant bands [19] results in well-shaped peaks in the Raman response observed at the same frequencies in A_{1g} and E_g symmetries, with the highest intensity in the A_{1g} symmetry.

Optical conductivity also shows a broad peak at around 100 meV [14]. In inversion-symmetric crystals Raman measurements should only probe electronic transitions from bands of the same parity while infrared is limited to bands of different parity. Here the mixed parity of the hybridized $5d$-$4f$ orbitals in SmB_6 allows this transition to appear in both responses, as also expected from the Raman response of a system with strong electronic correlations [38,39].

An increase of the number of Sm vacancies within 1% between the Al Flux-SmB_6 and FZ SmB_6-Def samples does not affect the 100 meV feature; however it results in an increase of the in-gap spectral weight and the respective decrease of the 41 meV band (Fig. 3). This suggests that the hybridization gap is not opened completely in the presence of 1% of Sm vacancies.

For the Al Flux-SmB_6 sample the sharp in-gap excitations are observed in the region of 16–17 meV in E_g and T_{2g} symmetries. The most intense feature belongs to the E_g symmetry, which probes electronic excitation at the X point of the BZ. A similar narrow in-gap excitation was observed by neutron scattering at finite-momentum transfers with scattering intensity at the X and R points of the BZ [20]. Raman scattering probes direct electronic transitions, and thus the energy of these excitation of 16 meV is higher than that observed in neutron scattering at 14 meV. Recently, this feature

was interpreted in terms of scattering on the excitonic level formed by electrons of hybridized bands in the gap as a result of strong electron-electron correlations and protected from decay by the hybridization gap [41]. The low linewidth of the excitonic features observed in the Al Flux-SmB_6 sample (0.5 meV) is evidence of a long lifetime due to protection from decay by the hybridization gap.

The parameters of the in-gap exciton reveal the difference between the two samples with the least number of Sm vacancies, Al Flux-SmB_6 and FZ SmB_6-Pure. In FZ SmB_6-Pure spectra the exciton feature shows lower intensity, and is widened to 1.7 meV (Fig. 5). The widening of the feature on the increase of the number of vacancies indicates the faster exciton decay which is evidence that electronic impurity states are present within the gap. This shows that even with the number of Sm vacancies below 1% but still distinguishable by Raman scattering, as in FZ SmB_6-Pure, some electronic states can be present in the hybridization gap and lead to metallic bulk response. No exciton features are detected in the spectra of FZ SmB_6-Def since the gap is not fully opened in this material.

The multiple exciton features of T_{2g} symmetry for the Al Flux-SmB_6 sample (Fig. 5; Table II) cannot be explained by pure electronic response. The previous work [27,28] proposes an alternative model for the multiple excitonic features which appear as a result of a splitting of crystal field levels by coupling with phonons [42]. According to the model, the feature at 16 meV in E_g symmetry has a dominant electronic contribution, which agrees with a pure electronic interpretation, while multiple exciton-related features in T_{2g} symmetry have a dominant phonon contribution [28].

Our results show that the most stoichiometric samples (Al Flux-SmB_6 in this study) possess a robust hybridization gap which makes the TKI state possible, with the in-gap exciton being evidence of the TKI state [20]. Not only 1% Sm vacancies suppress the development of the hybridization gap and thus would eliminate the TKI state, but even the lower—but detectable by Raman scattering—number of vacancies leads to the presence of electronic states in the gap, which can also be disruptive for the TKI state. While introduction of Sm vacancies is a way to change Sm valence and to explore the phase diagram proposed in Ref. [3], the largest number of vacancies in the studied samples of about 1% is too small to change the Sm average valence by values that would lead to tuning the system out of the TKI state. This result suggests that the TKI state in SmB_6 is extremely sensitive to disorder and variation of valence through the introduction of Sm vacancies [3].

The presence of Sm vacancies can introduce doping, but the effects of disorder also can be important. To probe the exact mechanism of an effect of Sm vacancies on the metallic low-temperature response of SmB_6 one needs to use frequency-dependent optical techniques which in contrast to Raman scattering have an ability to directly probe the bulk charge carriers.

Our Raman results for the FZ-grown samples are mirrored by transport measurements which show smaller $\rho(2\text{ K})/\rho(300\text{ K})$ ratio and an absence of a low-temperature plateau for the sample with 1% Sm vacancies (FZ SmB_6-Def) [21]. However, our results suggest that, even for the more insulating sample FZ SmB_6-Pure where the resistivity plateau is observed, the electronic states are present in the gap. Thus our work demonstrates that conclusions on the TKI state in SmB_6 samples cannot be drawn without a very careful characterization of the number of Sm vacancies. For example, in Ref. [22] where a 3D metallic Fermi surface was demonstrated for SmB_6, Sm stoichiometry was only verified down to the 1% level. This can still allow bulk metallic response due to a not fully opened hybridization gap, as seen from our results.

V. CONCLUSIONS

In this work we demonstrate that the possibility of a TKI state in SmB_6 is limited to the most stoichiometric samples. This is essential, since the presence of a very low number of Sm vacancies is typical for this material. We study three samples of SmB_6 with different numbers of vacancies, from nondetectable to 1%, using the Raman scattering technique. The increasing number of Sm vacancies results in local symmetry breaking, which is observed in Raman spectra as an increasing intensity of the Raman-forbidden phonon at 10 meV associated with Sm movement.

On cooling, in the electronic Raman response of SmB_6 we observe a shift of the spectral weight to higher frequencies due to opening of the hybridization gap. For the stoichiometric SmB_6 the two electronic maxima at 100 and 41 meV appear at 130 and 50 K in A_{1g} and E_g symmetries. Basing on the recent electronic structure calculations, we assign the features to the excitations between the bands which are formed due to hybridization between $5d$ and $4f$ orbitals. Below 30 K we observe the narrow features of the in-gap excitons, with the most intense one at 16 meV detected when probing the electronic transitions at the X point of the BZ. The extremely low linewidth of 0.5 meV suggests the long lifetime of the exciton protected from the decay by the hybridization gap. We conclude that in the most stoichiometric SmB_6 samples the hybridization gap is fully opened and the TKI state is possible.

The presence of less than 1% Sm vacancies leads to a decrease of the exciton lifetime through introducing electronic states in the gap. With the increase of the number of Sm vacancies up to approximately 1% the hybridization gap is filled with electronic states at the lowest measured temperature without a detectable change in the size of the gap, and the exciton is fully quenched. This would result in bulk conductivity and a breakdown of the TKI state due to the absence of a robust hybridization gap.

ACKNOWLEDGMENTS

We are grateful to C. Broholm, P. Nikolić, W. Fuhrman, J. Paglione, and N. P. Armitage for useful discussions. The work at IQM was supported by the US Department of Energy, Office of Basic Energy Sciences, Division of Material Sciences and Engineering, under Grant No. DE-FG02-08ER46544.

[1] M. Dzero, K. Sun, V. Galitski, and P. Coleman, Phys. Rev. Lett. **104**, 106408 (2010).

[2] M. Dzero, K. Sun, P. Coleman, and V. Galitski, Phys. Rev. B **85**, 045130 (2012).

[3] V. Alexandrov, M. Dzero, and P. Coleman, Phys. Rev. Lett. **111**, 226403 (2013).

[4] R. L. Cohen, M. Eibschütz, and K. W. West, Phys. Rev. Lett. **24**, 383 (1970).

[5] Z. Fisk, J. Sarrao, S. Cooper, P. Nyhus, G. Boebinger, A. Passner, and P. Canfield, Phys. B (Amsterdam, Neth.) **223-224**, 409 (1996).

[6] S. Wolgast, Ç. Kurdak, K. Sun, J. W. Allen, D.-J. Kim, and Z. Fisk, Phys. Rev. B **88**, 180405 (2013).

[7] W. A. Phelan, S. M. Koohpayeh, P. Cottingham, J. W. Freeland, J. C. Leiner, C. L. Broholm, and T. M. McQueen, Phys. Rev. X **4**, 031012 (2014).

[8] P. Syers, D. Kim, M. S. Fuhrer, and J. Paglione, Phys. Rev. Lett. **114**, 096601 (2015).

[9] Z.-H. Zhu, A. Nicolaou, G. Levy, N. P. Butch, P. Syers, X. F. Wang, J. Paglione, G. A. Sawatzky, I. S. Elfimov, and A. Damascelli, Phys. Rev. Lett. **111**, 216402 (2013).

[10] D. Kim, S. Thomas, T. Grant, J. Botimer, Z. Fisk, and J. Xia, Sci. Rep. **3**, 3150 (2013).

[11] J. Jiang, S. Li, T. Zhang, Z. Sun, F. Chen, Z. Ye, M. Xu, Q. Ge, S. Tan, X. Niu, M. Xia, B. Xie, Y. Li, X. Chen, H. Wen, and D. Feng, Nat. Commun. **4**, 3010 (2013).

[12] G. Travaglini and P. Wachter, Phys. Rev. B **29**, 893 (1984).

[13] H. Ohta, R. Tanaka, M. Motokawa, S. Kunii, and T. Kasuya, J. Phys. Soc. Jpn. **60**, 1361 (1991).

[14] T. Nanba, H. Ohta, M. Motokawa, S. Kimura, S. Kunii, and T. Kasuya, Phys. B (Amsterdam, Neth.) **186-188**, 440 (1993).

[15] B. Gorshunov, N. Sluchanko, A. Volkov, M. Dressel, G. Knebel, A. Loidl, and S. Kunii, Phys. Rev. B **59**, 1808 (1999).

[16] K. Flachbart, K. Gloos, E. Konovalova, Y. Paderno, M. Reiffers, P. Samuely, and P. Švec, Phys. Rev. B **64**, 085104 (2001).

[17] I. Frankowski and P. Wachter, Solid State Commun. **41**, 577 (1982).

[18] V. N. Antonov, B. N. Harmon, and A. N. Yaresko, Phys. Rev. B **66**, 165209 (2002).

[19] F. Lu, J. Zhao, H. Weng, Z. Fang, and X. Dai, Phys. Rev. Lett. **110**, 096401 (2013).

[20] W. T. Fuhrman, J. Leiner, P. Nikolić, G. E. Granroth, M. B. Stone, M. D. Lumsden, L. DeBeer-Schmitt, P. A. Alekseev, J.-M. Mignot, S. M. Koohpayeh, P. Cottingham, W. A. Phelan, L. Schoop, T. M. McQueen, and C. Broholm, Phys. Rev. Lett. **114**, 036401 (2015).

[21] W. A. Phelan, S. M. Koohpayeh, P. Cottingham, J. C. Leiner, M. D. Lumsden, X. P. Wang, C. Hoffmann, M. A. Siegler, and T. M. McQueen, Sci. Rep. **6**, 20860 (2016).

[22] B. S. Tan, Y.-T. Hsu, B. Zeng, M. C. Hatnean, N. Harrison, Z. Zhu, M. Hartstein, M. Kiourlappou, A. Srivastava, M. D. Johannes, T. P. Murphy, J.-H. Park, L. Balicas, G. G. Lonzarich, G. Balakrishnan, and S. E. Sebastian, Science **349**, 287 (2015).

[23] M. Valentine *et al.* (unpublished).

[24] T. Kasuya, K. Kojima, and M. Kasaya, in *Valence Instabilities and Related Narrow-Band Phenomena* (Springer, Boston, MA, 1977), pp. 137–152.

[25] N. Ogita, S. Nagai, N. Okamoto, M. Udagawa, F. Iga, M. Sera, J. Akimitsu, and S. Kunii, Phys. Rev. B **68**, 224305 (2003).

[26] I. Morke, V. Dvorak, and P. Wachter, Solid State Commun. **40**, 331 (1981).

[27] P. Nyhus, S. L. Cooper, Z. Fisk, and J. Sarrao, Phys. Rev. B **52**, R14308 (1995).

[28] P. Nyhus, S. L. Cooper, Z. Fisk, and J. Sarrao, Phys. Rev. B **55**, 12488 (1997).

[29] N. Ogita, S. Nagai, M. Udagawa, F. Iga, M. Sera, T. Oguchi, J. Akimitsu, and S. Kunii, Phys. B (Amsterdam, Neth.) **359-361**, 941 (2005).

[30] R. Shuker and R. W. Gammon, Phys. Rev. Lett. **25**, 222 (1970).

[31] P. A. Alekseev, A. S. Ivanov, B. Dorner, H. Schober, K. A. Kikoin, A. S. Mishchenko, V. N. Lazukov, E. S. Konovalova, Y. B. Paderno, A. Y. Rumyantsev, and I. P. Sadikov, Europhys. Lett. **10**, 457 (1989).

[32] P. A. Alekseev *et al.*, Phys. Usp. **58**, 330 (2015).

[33] M. Cardona and G. Guntherodt, *Light Scattering in Solids. II. Basic Concepts and Instrumentation* (Springer-Verlag, Berlin Heidelberg, 1982), Introduction.

[34] P. Lemmens, A. Hoffmann, A. Mishchenko, M. Talantov, and G. Gntherodt, Phys. B (Amsterdam, Neth.) **206-207**, 371 (1995).

[35] M. V. Klein, Phys. Rev. B **24**, 4208 (1981).

[36] H. Wipf, M. V. Klein, and W. S. Williams, Phys. Status Solidi B **108**, 489 (1981).

[37] E. Burstein, D. Mills, and R. Wallis, Phys. Rev. B **4**, 2429 (1971).

[38] J. K. Freericks, T. P. Devereaux, M. Moraghebi, and S. L. Cooper, Phys. Rev. Lett. **94**, 216401 (2005).

[39] J. K. Freericks and T. P. Devereaux, Phys. Rev. B **64**, 125110 (2001).

[40] T. P. Devereaux and R. Hackl, Rev. Mod. Phys. **79**, 175 (2007).

[41] W. T. Fuhrman and P. Nikolić, Phys. Rev. B **90**, 195144 (2014).

[42] P. Thalmeier and P. Fulde, Phys. Rev. Lett. **49**, 1588 (1982).